Am J Transl Res 2025;17(8):6414-6424
www.ajtr.org /ISSN:1943-8141/AJTR0166900

Original Article

DUSP1 alleviates LPS-induced acute lung injury by inhibiting the SHP2-JNK axis and mitochondrial apoptosis

Sheng Chen[1,2], Yunnan Hu[1,2], Lingfeng Li[1,2], Jiaxin Zhang[1,2], Rongda Huang[1,2], Mirong Tang[1,2]

[1]Department of Cardiovascular Surgery, Fujian Medical University Union Hospital, Fuzhou 350001, Fujian, China; [2]Key Laboratory of Cardio-Thoracic Surgery (Fujian Medical University), Fujian Province University, Fuzhou 350001, Fujian, China

Received June 18, 2025; Accepted July 31, 2025; Epub August 15, 2025; Published August 30, 2025

Abstract: Background: Lipopolysaccharide (LPS) induces acute lung injury (ALI), a condition characterized by oxidative stress, inflammation, and apoptosis, ultimately leading to respiratory failure. Dual-specificity phosphatase 1 (DUSP1), a key regulator of MAPK signaling, may offer protection against inflammatory damage. Objective: This study aimed to investigate the protective effects of DUSP1 overexpression against LPS-induced inflammatory injury and to explore the underlying molecular mechanisms using both *in vitro* and *in vivo* models. Methods: Cellular and murine ALI models were established using LPS. DUSP1 was overexpressed via plasmid transfection for *in vitro* experiments and viral vectors for *in vivo* studies. Cell viability, apoptosis, reactive oxygen species (ROS), and pro-inflammatory cytokine levels (IL-1β, IL-6, TNF-α) were assessed. In mice, lung injury was evaluated through bronchoalveolar lavage fluid (BALF) analysis, lung mechanics, and histopathology. DUSP1-SHP2 interactions were predicted using bioinformatics and validated through co-immunoprecipitation. JNK pathway activation was analyzed by Western blotting, and dual-luciferase reporter assays confirmed the regulatory interaction between DUSP1 and SHP2. Results: In vitro, DUSP1 overexpression significantly enhanced cell viability while reducing apoptosis, ROS, malondialdehyde (MDA), and inflammatory cytokines in LPS-stimulated cells. In vivo, DUSP1 overexpression substantially alleviated LPS-induced lung injury, evidenced by decreased BALF protein, reduced lung water content, lower airway resistance, improved pulmonary function, and less tissue damage. Mechanistically, DUSP1 directly interacted with SHP2, inhibiting its phosphorylation, which in turn suppressed the phosphorylation of p53 and JNK. DUSP1 overexpression also downregulated PINK1/Parkin-mediated mitophagy, key pro-apoptotic proteins (Cytochrome C, Caspase-3, Bax), and the NLRP3 inflammasome. Anisomycin treatment reversed these protective effects, confirming the dependence of DUSP1's protective action on JNK pathway inhibition. Conclusion: DUSP1 overexpression alleviates LPS-induced lung inflammation and injury by targeting the SHP2-JNK axis and restoring mitochondrial homeostasis. These findings position DUSP1 as a promising therapeutic target for inflammatory lung disorders.

Keywords: DUSP1, SHP-2, JNK/P53/NLRP3 signaling pathway, mitochondrial autophagy, septic acute lung injury

Introduction

Acute lung injury (ALI) and its more severe form, acute respiratory distress syndrome (ARDS), are critical pulmonary disorders with high morbidity and mortality [1]. These syndromes are marked by extensive alveolar epithelial disruption, pulmonary fluid accumulation, elevated oxidative stress, and an uncontrolled inflammatory response. Among the etiological factors, lipopolysaccharide (LPS), a bacterial endotoxin, is frequently employed to replicate the pathophysiological features of ALI in experimental models, due to its potent ability to induce innate immune activation and cytokine amplification, culminating in respiratory failure [2]. Despite advancements in intensive care management, effective pharmacological interventions that address the core mechanisms of ALI pathogenesis are still lacking.

Central to LPS-induced tissue injury is the activation of mitogen-activated protein kinase (MAPK) pathways, which orchestrate a variety of stress responses [3]. Within this family, the c-Jun N-terminal kinase (JNK) cascade is particularly implicated in promoting apoptotic cell death, oxidative imbalance, and inflammatory

https://doi.org/10.62347/QAUM4023

mediator release in pulmonary tissues [4]. Dual-specificity phosphatase 1 (DUSP1, also known as MKP-1), a key endogenous suppressor of MAPK signaling, modulates these responses by dephosphorylating JNK, p38, and ERK [2, 5]. The study by Pu et al. found that Ginsenoside Rb1 alleviates heart failure by modulating the DUSP-1 - TMBIM-6 - VDAC1 axis, thereby orchestrating crosstalk between inflammation and mitochondrial quality control [6]. Although DUSP1 has been recognized for its inducibility under inflammatory stimuli and its potential to temper immune activation [7], the mechanistic basis of its interaction with JNK signaling and its influence on mitochondrial stability under inflammatory stress remains incompletely defined.

Emerging evidence highlights SHP2, a non-receptor protein tyrosine phosphatas, as a crucial player in various cell signaling pathways activated by growth factors, cytokines, and hormones that regulate cell survival, growth and differentiation [8, 9]. SHP2 acts as a pivotal upstream regulator of MAPK signaling and facilitates JNK pathway activation [10, 11]. Aberrant phosphorylation of SHP2 has been associated with heightened pulmonary injury, possibly by promoting JNK-driven mitochondrial dysfunction, suppressing mitophagy, and enhancing pro-apoptotic signaling cascades [12, 13]. However, the potential interaction between DUSP1 and SHP2 in modulating this signaling axis in ALI remains to be clarified.

This study aims to investigate the functional roles of DUSP1 in LPS-induced lung injury, using both cell-based systems and a murine ALI model. Elucidating this regulatory framework may offer mechanistic insight and therapeutic direction for the treatment of inflammatory lung disease.

Materials and methods

Materials and instruments

C57BL/6 mice (5-7 weeks old) were purchased from Beijing Vital River Laboratory Animal Technology Co., Ltd. The animal experiments in this study were approved by the Ethics Committee of the Union Hospital of Fujian Medical University (approval number: 2021KJT063). LPS was purchased from Solabio, MLE-12 cells were purchased from Wuhan Procell, and fetal bovine serum was sourced from Gibco (USA). RIPA lysis buffer and PVDF membrane IPVH20200 were obtained from American Millipore, while pre-stained protein marker, skim milk powder, PBS, 4% paraformaldehyde solution, 0.25% trypsin digestion solution, Hi TransGP infection enhancer, DUSP1-OE, PHPS1, and a 95% air, 5% CO_2 cell culture incubator were purchased from Themo Fisher (USA). The transilluminator and imaging system, as well as Western blot electrophoresis apparatus were all purchased from Bio-Rad (USA).

Establishment and grouping of mouse models

Male C57BL/6 mice (5-7 weeks old) were purchased from Beijing Vital River Laboratory Animal Technology Co., Ltd. and housed under specific pathogen-free (SPF) conditions for acclimatization. After one week of adaptation, the mice were randomly divided into three groups (n = 3 per group): normal control (NC), lipopolysaccharide-treated (LPS), and LPS combined with DUSP1 overexpression (LPS+DUSP1-OE). Septic lung injury was induced in the LPS and LPS+DUSP1-OE groups via a single intraperitoneal injection of LPS (5 mg/kg). After successful model establishment, mice in the LPS group received daily intraperitoneal injections of normal saline (0.9% NaCl, 3 mg/kg/day). In contrast, mice in the LPS+DUSP1-OE group were administered a single intraperitoneal injection of a DUSP1-overexpressing lentiviral vector (1×10^8 transduction units per mouse). Mice in the NC group received equivalent volumes of sterile saline without LPS or vector administration.

Collection, processing and determination of BALF protein concentration

Bronchoalveolar lavage fluid (BALF) was collected by surgically exposing the trachea at the cervical level. A sterile 1 mL aliquot of phosphate-buffered saline (PBS) was gently infused into the left lung via a syringe inserted through the tracheal incision. The lavage procedure was repeated three times to ensure adequate sampling of the alveolar compartment. The collected BALF was pooled and immediately subjected to centrifugation at 800×g for 10 minutes to separate cellular components. The resulting supernatant was harvested, and total protein concentration was quantified using a bicinchoninic acid (BCA) assay kit (Beyotime, Shanghai, China).

ELISA

BALF samples were centrifuged at 1500 rpm for 5 minutes at 4°C to separate cellular components. The resulting cell pellet was resuspended in 0.5 mL of PBS, while the cell-free supernatant was collected for downstream analysis. Levels of inflammatory cytokines, including MDA, IL-1β, IL-10, and TNF-α, were quantified using enzyme-linked immunosorbent assay (ELISA) kits according to the manufacturer's instructions (Beyotime, Shanghai, China).

Lung wet-to-dry ratio

Pulmonary edema was assessed by calculating the lung wet-to-dry (W/D) weight ratio. Following euthanasia, the left lung was carefully excised, blotted to remove excess surface fluid, and immediately weighed to record the wet weight. The tissue was then dried in an oven at 60°C for 72 hours until a stable dry weight was obtained. The W/D ratio was calculated by dividing the wet weight by the dry weight, serving as an indicator of lung water content.

Intracellular ROS measurement

Intracellular reactive oxygen species (ROS) levels were quantified using the fluorescent probe 2',7'-dichlorofluorescein diacetate (DCFH-DA; 10 μmol/L; Beyotime, Shanghai, China). Cells were seeded into 24-well plates and incubated with DCFH-DA at 37°C for 30 minutes in the dark. After incubation, cells were washed three times with PBS to remove unincorporated dye. The fluorescence intensity of the oxidized product (DCF) was measured using a microplate reader with excitation and emission wavelengths set at 488 nm and 525 nm, respectively. ROS levels were normalized to total protein content to account for variations in cell density across samples.

Lung function measurements

Lung function was measured using the Buxco Lung Function Test System. Airway resistance, lung compliance, and lung ventilation were calculated as follows.

Airway resistance: $Ri = \frac{P_{peak} - P_{plat}}{Flow}$, where P_{peak} is the highest pressure during ventilator delivery, P_{plat} is the plateau pressure, and Flow is the gas flow velocity.

Lung compliance: $Cdyn = \frac{\triangle V}{\triangle P}$, where ΔV is the volume change and ΔP is the pressure change.

Pulmonary ventilation: *VE = respiratory rate × tidal volume*.

HE staining experiment

Following tissue collection, paraffin-embedded sections were deparaffinized by sequential immersion in xylene I (10 minutes) and xylene II (2 minutes). Rehydration was performed through a graded ethanol series: absolute ethanol I (5 minutes), absolute ethanol II (5 minutes), 95% ethanol (5 minutes), 85% ethanol (5 minutes), and 70% ethanol (5 minutes), followed by a 5-minute rinse in distilled water. Hematoxylin staining was performed for 4 minutes, after which the sections were rinsed under running tap water for 10 minutes. Nuclei were briefly differentiated using hydrochloric acid in ethanol (3 seconds) and rinsed again for 10 minutes. Counterstaining with eosin was carried out for 25 seconds to 1 minute, followed by dehydration, clearing, and mounting using neutral resin. The slides were air-dried and examined under a light microscope.

Protocol for cell culture and experimental design

For *in vitro* experiments, MLE-12 murine lung epithelial cells were seeded into 24-well plates at a density of 2×10^7 cells/mL (500 μL/well) and incubated at 37°C for 24 hours. To enhance transduction efficiency, 20 μL of 25 × HiTransGP infection enhancer was added per well. The lentiviral vector was applied based on the calculated viral dose using the formula: viral load = (multiplicity of infection × number of cells)/viral titer. The lentiviral solution was mixed with complete culture medium and incubated for 16 hours at 37°C. After incubation, the medium was replaced, and the cells were cultured until approximately 80% confluency. Transfection efficiency was evaluated via fluorescence microscopy, and overexpression of the target protein was confirmed by Western blot, verifying the successful generation of MLE-12 cells with stable DUSP1 overexpression.

Flow cytometric analysis of apoptosis

Apoptotic cell death was quantified by Annexin V-FITC and propidium iodide (PI) double staining followed by flow cytometry. MLE-12 cells were collected, washed twice with cold PBS, and resuspended in 1 × binding buffer. Each sample was incubated with 5 μL Annexin V-FITC and 5 μL PI (Annexin V-FITC/PI Apoptosis Detection Kit; Beyotime, Shanghai, China) for 15 minutes in the dark at room temperature. Samples were then analyzed using a BD FACSCanto II flow cytometer, and data were processed with FlowJo software. The proportions of early apoptotic (Annexin V^+/PI^-) and late apoptotic or necrotic (Annexin V^+/PI^+) cells were calculated.

Cell viability assay

Cell viability was assessed using the Cell Counting Kit-8 (CCK-8; Dojindo, Japan) in accordance with the manufacturer's instructions. MLE-12 cells were plated in 96-well plates at a density of 5×10^3 cells per well and allowed to adhere overnight. After 72 hours of treatment under the specified experimental conditions, 10 μL of CCK-8 reagent was added to each well, followed by incubation at 37°C for 2 hours. Absorbance was measured at 450 nm using a microplate reader. Viability was expressed as a percentage relative to untreated control.

Western blotting

Total protein was extracted from MLE-12 cells in each experimental group using a commercially available lysis kit, followed by quantification using a BCA protein assay. Equal amounts of protein were resolved via SDS-PAGE and transferred onto polyvinylidene difluoride (PVDF) membranes. Membranes were blocked at room temperature for 2 hours and then incubated overnight at 4°C with the following primary antibodies: DUSP1 (1:2,000), SHP2 (1:2,000), phospho-SHP2 (1:20,000), P53 (1:2,000), phospho-JNK (1:2,000), PINK1 (1:20,000), Parkin (1:2,000), cytochrome c (1:2,000), caspase-3 (1:20,000), Bax (1:2,000), NLRP3 (1:2,000), and GAPDH (1:10,000) (all from specified commercial sources). After washing, membranes were incubated with goat anti-rabbit HRP-conjugated secondary antibody (1:2,000) at 37°C for 90 minutes. All antibodies were purchased from Abcam, USA. Protein bands were visualized using chemiluminescence, and densitometric analysis was performed using ImageJ software to quantify relative protein expression levels, normalized to GAPDH.

Target prediction

To investigate the potential interaction between DUSP1 and SHP2 (PTPN11), protein-protein interaction (PPI) data were collected from multiple publicly available databases, including STRING (version 11.0), BioGRID, GeneMANIA, and ENCORI. DUSP1 was used as the query gene, and putative interacting proteins were retrieved based on experimental evidence, database annotations, and prediction algorithms.

The retrieved interaction pairs were imported into Cytoscape (version 3.7.1) to construct a DUSP1-centered PPI network. Network topology analysis was performed using the CytoNCA plugin to evaluate node degree, betweenness, and closeness.

Dual-luciferase reporter gene assay

To validate the direct regulatory relationship between DUSP1 and SHP2, a dual-luciferase reporter assay was performed. Wild-type (WT) and mutant (MUT) sequences of the predicted DUSP1-responsive region within the SHP2 promoter were cloned into the pmirGLO dual-luciferase reporter vector (Promega, USA). HEK293T cells were seeded into 24-well plates and co-transfected with either WT or MUT reporter plasmids along with a lentiviral vector overexpressing DUSP1 or control using Lipofectamine 2000 (Invitrogen, USA). After 24 hours, luciferase activity was measured using the Dual-Luciferase® Reporter Assay System (Promega), and the firefly luciferase activity was normalized to Renilla luciferase. The relative luciferase activity (FLUC/RLUC) was compared between groups to determine the regulatory effect of DUSP1.

Statistical data analysis

All data were analyzed using GraphPad Prism 9 software. Results were expressed as mean ±

standard deviation (SD). Comparisons between two groups were performed using unpaired two-tailed Student's t-test. For comparisons involving more than two groups, one-way analysis of variance (ANOVA) followed by Tukey's post-hoc test was used to determine significant differences among the groups. A p-value < 0.05 was considered statistically significant. Statistical significance was denoted as P < 0.05, *P < 0.01, and P < 0.001, where applicable.

Results

DUSP1 overexpression alleviated LPS-induced oxidative stress, apoptosis, and inflammation in vitro

LPS stimulation markedly suppressed endogenous DUSP1 protein expression, which was successfully reversed via targeted overexpression (**Figure 1A**). Restoring DUSP1 levels conferred profound cytoprotection against the LPS challenge. Specifically, cells overexpressing DUSP1 exhibited a significantly enhanced survival rate compared to the controls (**Figure 1B**), coupled with a substantial reduction in apoptosis, as quantified by flow cytometry (**Figure 1C**). This protective effect was mechanistically linked to the mitigation of cellular stress, as evidenced by a substantial reduction in reactive oxygen species (ROS) accumulation in DUSP1-overexpressing cells (**Figure 1D**). Additionally, the inflammatory response elicited by LPS was significantly reduced, as evidenced by the diminished expression of pro-inflammatory cytokines IL-1β, IL-6, and TNF-α (**Figure 1E**). Collectively, these findings establish that DUSP1 counteracts LPS-induced cellular injury by concurrently inhibiting apoptosis, oxidative stress, and the inflammatory cascade.

DUSP1 overexpression ameliorated LPS-induced lung injury and dysfunction in mice

The in vivo protective effects of DUSP1 were subsequently validated in a murine model of LPS-induced acute lung injury. LPS challenge precipitated a sharp rise in bronchoalveolar lavage fluid (BALF) protein levels, indicating impaired alveolar-capillary barrier integrity, which was markedly attenuated by DUSP1 overexpression (**Figure 2A**). This restoration of barrier function was further evidenced by a significant reduction in lung water content, indicating that DUSP1 effectively mitigated the formation of pulmonary edema (**Figure 2B**). Functionally, the severe impairment of pulmonary ventilation and airway mechanics - characterized by decreased compliance and elevated maximal respiratory resistance - observed in the LPS-treated cohort was substantially reversed in animals overexpressing DUSP1 (**Figure 2C-E**). Furthermore, DUSP1 overexpression robustly suppressed the systemic oxidative stress, as evidenced by the significantly lower levels of malondialdehyde (MDA) (**Figure 2F**). Histopathological examination of lung tissue corroborated these functional and biochemical data, revealing that DUSP1 markedly ameliorated the extensive inflammatory infiltration and structural damage inflicted by LPS (**Figure 2G**). Taken together, these results compellingly demonstrate that DUSP1 protects against LPS-induced lung injury by preserving pulmonary mechanics and attenuating edema, oxidative stress, and inflammation.

DUSP1 overexpression downregulated SHP2 phosphorylation and interacted directly with SHP2

To delineate the molecular mechanism by which DUSP1 exerts its anti-inflammatory effects, we investigated its functional relationship with SHP2, a key upstream regulator of MAPK signaling. In *silico* analyses using multiple PPI databases (including STRING, BioGRID, and GeneMANIA) consistently predicted a direct regulatory link between DUSP1 and SHP2 (PTPN11). Experimentally, we found that LPS stimulation induced robust phosphorylation of SHP2. While DUSP1 overexpression did not alter total SHP2 levels, it potently inhibited LPS-induced SHP2 phosphorylation by approximately 40% (**Figure 3A**), suggesting a direct regulatory effect. This hypothesis was confirmed using co-immunoprecipitation (Co-IP) assays, which provided unequivocal evidence of a physical association between the two proteins, as Myc-SHP2 was efficiently pulled down with FLAG-DUSP1 (**Figure 3B**). To verify a direct physical interaction between DUSP1 and SHP2, co-immunoprecipitation (Co-IP) assays were conducted. FLAG-tagged DUSP1 efficiently pulled down Myc-tagged SHP2, confirming the existence of a specific protein - protein interac-

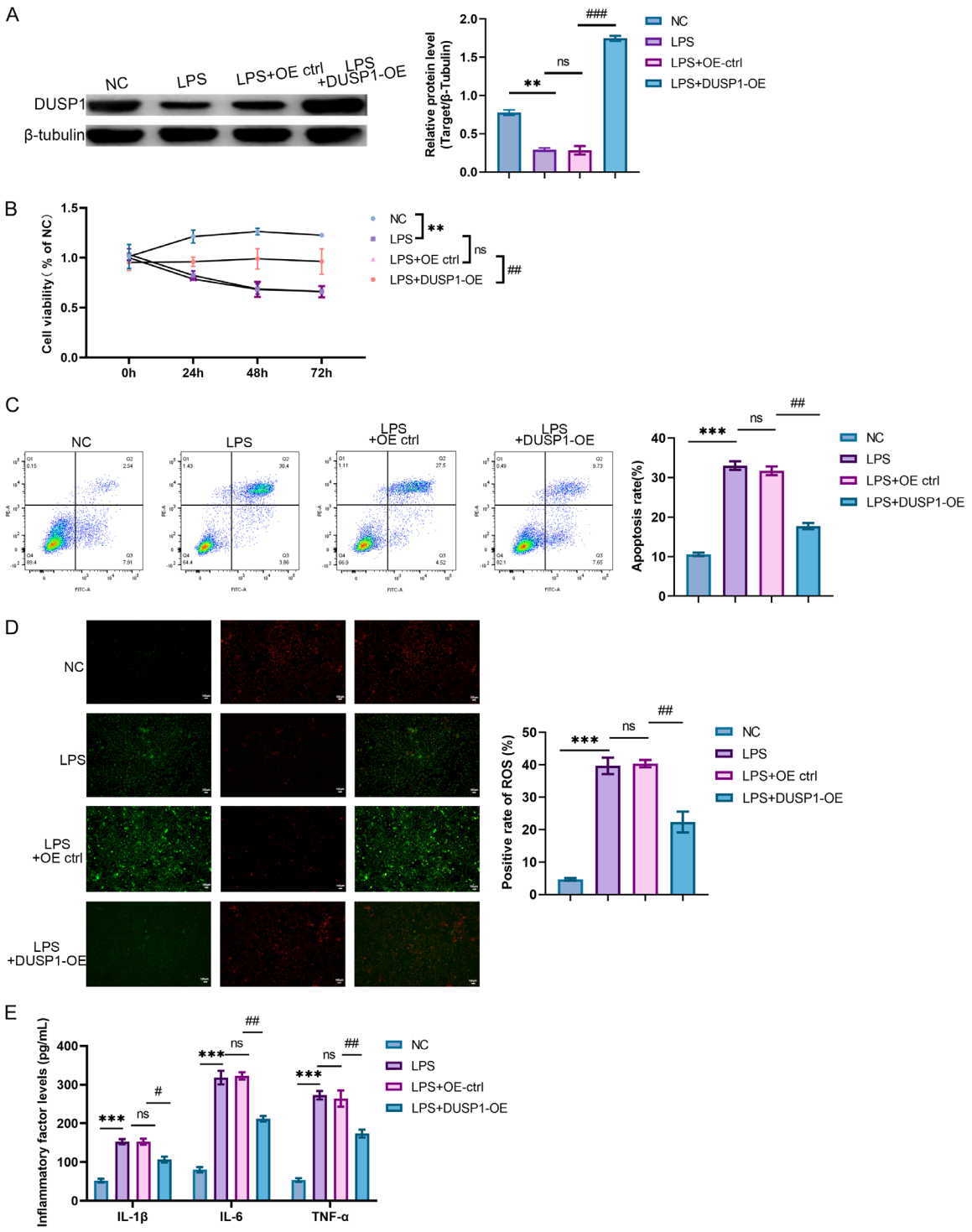

Figure 1. Impact of DUSP1 overexpression on cell viability, apoptosis, ROS production, oxidative stress, and inflammation in LPS-treated cells. A. Western blot analysis showing DUSP1 expression levels across experimental groups. B. Cell viability was assessed at multiple time points following LPS exposure, with or without DUSP1 overexpression. C. Flow cytometric detection of apoptosis rates in each group. D. ROS levels were detected using fluorescence imaging and quantified as the positive rate (10×). E. ELISA quantification of inflammatory cytokines IL-1β, IL-6, and TNF-α. Data are presented as mean ± SD. **P < 0.01, ***P < 0.001, NC vs. LPS; ns, LPS vs. LPS+OE-ctrl; #P < 0.05, ##P < 0.01, ###P < 0.01, LPS+OE-ctrl vs. LPS+DUSP1-OE. Scale bar 100 μm.

tion (**Figure 3C**). Furthermore, a dual-luciferase reporter assay was performed to evaluate the functional relevance of this interaction. Compared to the control, DUSP1 overexpression

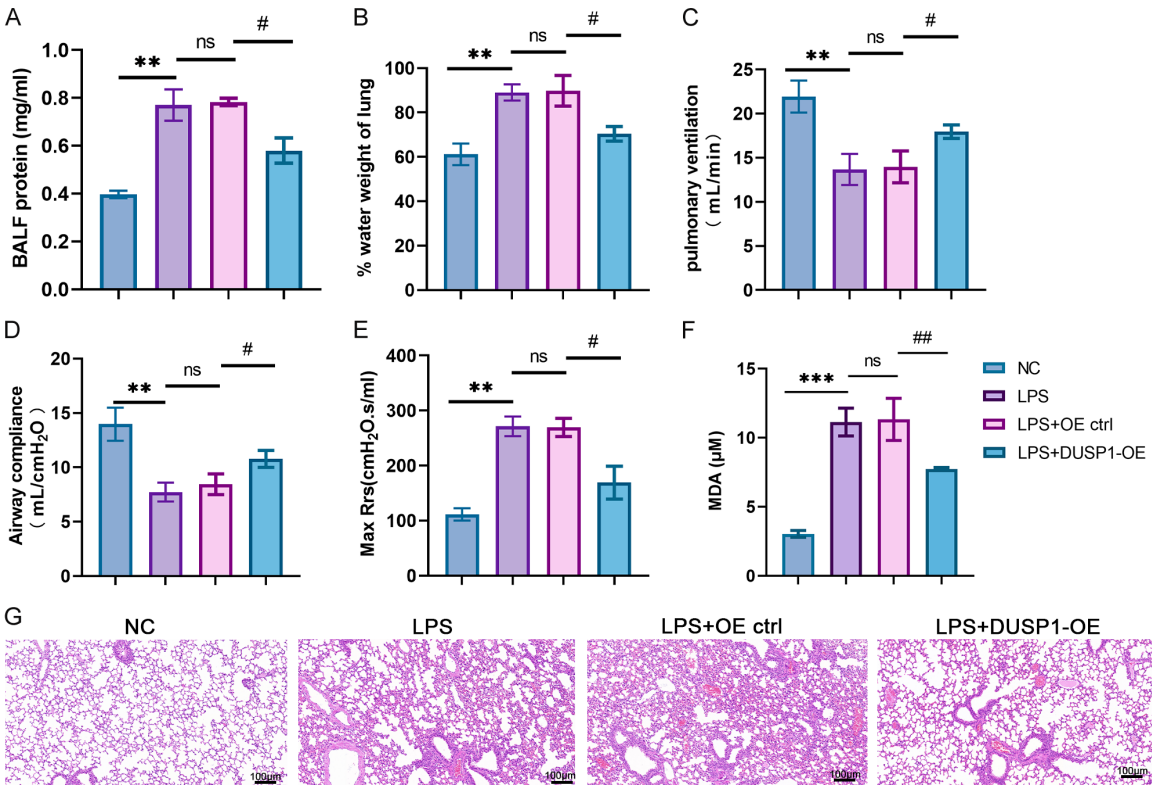

Figure 2. DUSP1 overexpression improved pulmonary function and reduced histological injury in LPS-induced lung injury. A. BALF protein concentration indicating alveolar-capillary barrier integrity. B. Lung water content expressed as percent wet lung weight. C. Pulmonary ventilation capacity across groups. D. Airway compliance (mL/cmH_2O) indicating lung elasticity. E. Maximum respiratory system resistance (Max Rrs). F. Malondialdehyde (MDA) levels in lung tissue. G. Representative H&E-stained lung sections showing histopathological changes across treatment groups. Data are presented as mean ± SD. **P < 0.01, ***P < 0.001, NC vs. LPS; ns, LPS vs. LPS+OE-ctrl; #P < 0.05, ##P < 0.01, ###P < 0.01, LPS+OE-ctrl vs. LPS+DUSP1-OE. Scale bar 100 μm.

significantly reduced luciferase activity driven by the wild-type SHP2 reporter construct, whereas no change was observed in the mutant construct lacking the DUSP1-responsive domain, indicating that the inhibitory effect of DUSP1 on SHP2 is domain-specific (**Figure 3D**). The specificity of this regulatory interaction was further validated through mutational analyses in a dual-luciferase reporter assay, which demonstrated that the binding is dependent on specific protein domains. These results support a model in which DUSP1 directly binds to SHP2, suppressing its phosphorylation and dismantling a critical node in the proinflammatory signaling cascade.

DUSP1 protected lung cell inflammatory response by regulating SHP2/JNK signaling pathway

To confirm that the JNK signaling axis is the principal downstream mediator of DUSP1's protective actions, we conducted rescue experiments using anisomycin, a pharmacological activator of the JNK pathway. As hypothesized, activating JNK with anisomycin completely nullified the survival advantage conferred by DUSP1 overexpression, returning cell viability to the vulnerable levels observed with LPS treatment alone (**Figure 4A**). This reversal extended to key cellular stress responses; the potent suppression of pro-inflammatory cytokines (IL-1β, IL-6, TNF-α) and oxidative stress, indicated by MDA levels, was significantly counteracted by anisomycin (**Figure 4B**, **4C**). At the molecular level, Western blot analysis revealed that the DUSP1-mediated downregulation of phosphorylated JNK (p-JNK) and its key effector, p53, was reversed by anisomycin treatment (**Figure 4D**). Critically, this reactivation of the JNK/p53 axis led to the disruption of mitochondrial integrity and activation of apoptotic signaling. The ability of DUSP1 to preserve mitochon-

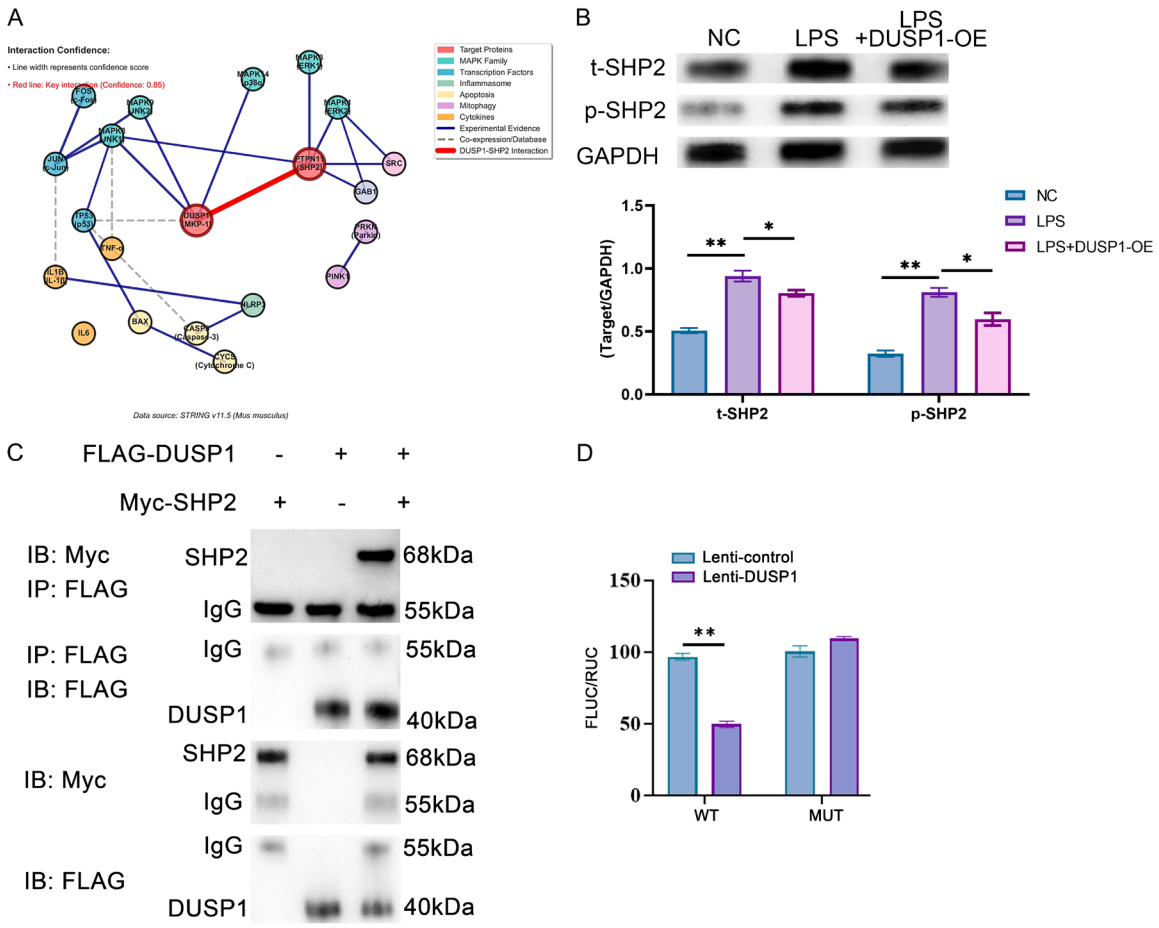

Figure 3. DUSP1 interacted with SHP2 and inhibited its phosphorylation. A. PPI protein interaction analysis. B. Western blot and quantification of total SHP2 (t-SHP2) and phosphorylated SHP2 (p-SHP2) levels in different treatment groups. C. Co-immunoprecipitation (Co-IP) analysis showing interaction between FLAG-tagged DUSP1 and Myc-tagged SHP2. D. The dual-luciferase reporter assays were performed to validate the interaction between DUSP1 and SHP2. Data are expressed as mean ± SD. *P < 0.05, **P < 0.01 compared with indicated groups.

drial integrity by inhibiting PINK1, Parkin, cytochrome c, and the NLRP3 inflammasome was abolished by anisomycin, leading to a resurgence in the levels of pro-apoptotic proteins Bax and cleaved caspase-3 (**Figure 4E**). These findings demonstrate that the cytoprotective effects of DUSP1 are mechanistically dependent on its inhibition of the JNK pathway, thereby preventing the execution of downstream mitochondrial dysfunction and apoptotic cell death.

Discussion

Sepsis continues to pose a formidable challenge in the emergency and intensive care medicine. Defined as a life-threatening organ dysfunction stemming from a dysregulated host response to infection, it is associated with morbidity and mortality rates exceeding 25% [14]. Among its severe complications, pulmonary impairment poses a considerable risk, with high mortality rates in septic patients. Therefore, elucidating the intricate underlying mechanisms of sepsis is indispensable for crafting targeted inhibitors and novel therapeutic strategies to mitigate pulmonary damage. This investigation reveals that DUSP1 overexpression alleviates the progression of sepsis-associated lung injury (SALI). Specifically, increased DUSP1 expression triggers a tripartite defense mechanism within pulmonary cells. Initially, it bolsters Fundc1-mediated mitophagy, although the precise molecular mechanisms remain to be fully elucidated. Subsequently, the resulting enhancement of mitochondrial autophagy is critical for maintaining mitochondrial function, with particular influence on cellular respiration

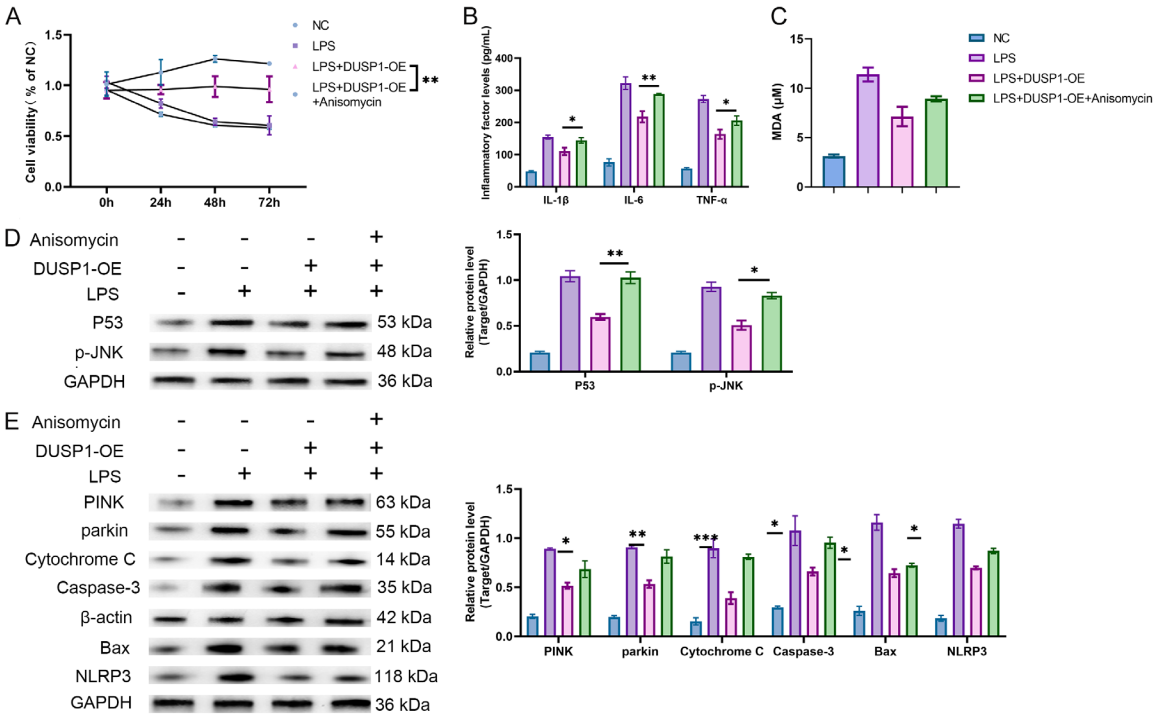

Figure 4. Electron microscopic observation of mitochondrial damage in lung tissue. A. Cell viability assessed at 0, 24, 48, and 72 h using CCK-8 assay in NC, LPS, LPS+DUSP1-OE, and LPS+DUSP1-OE+Anisomycin groups. B. ELISA quantification of inflammatory cytokines IL-1β, IL-6, and TNF-α. C. Malondialdehyde (MDA) levels as a marker of oxidative stress. D. Representative western blot and quantitative analysis of p53 and phosphorylated JNK (p-JNK) protein expression. GAPDH was used as an internal control. E. Western blot analysis and quantification of mitophagy-related proteins (PINK1, Parkin), mitochondrial apoptosis markers (Cytochrome C, Caspase-3, Bax), and inflammation-related protein NLRP3. β-actin or GAPDH served as loading controls. Data are presented as mean ± SD (n = 3); *P < 0.05, **P < 0.01, ***P < 0.001; ns, not significant (one-way ANOVA with Tukey's post hoc test).

and metabolic processes. Lastly, the amplified expression of DUSP1 concurrently mitigates inflammatory reactions and cellular demise [15]. Consequently, the strategic upregulation of DUSP1 emerges as an innovative approach to rehabilitate pulmonary function and restore mitochondrial equilibrium during sepsis.

The etiology of SALI is intricately connected to mitochondrial dysfunction. A heightened inflammatory milieu has been shown to correlate with aberrant mitochondrial division and atypical organelle morphology [16]. Notably, the PTPN11-encoded SHP2 protein, is recognized as an attenuator of inflammatory cascades within the NLRP3 inflammasome complex [17, 18]. Given that NLRP3 itself is implicated in oxidative stress and the activation of p53 - a pivotal factor in maintaining DNA integrity and mediating stress-induced senescence [19] - the functional role of p53 is particularly relevant in this context. Our research reveals that DUSP1 exerts a potent inhibitory effect on NLRP3 expression by disrupting the SHP2-JNK-p53 signaling axis. Overexpression of DUSP1 attenuated SHP2 phosphorylation, which subsequently led to the deactivation of JNK and p53, kinases known to promote NLRP3 activation. Importantly, treatment with anisomycin, a JNK activator, reversed the suppressive effect of DUSP1 on NLRP3, highlighting the dependence of this regulatory mechanism on the SHP2-JNK pathway. This DUSP1-driven regulatory mechanism stands in contrast to the pronounced NLRP3 upregulation observed following LPS challenge in acute lung injury. Collectively, these findings reveal a novel regulatory circuit where DUSP1 indirectly restrains NLRP3 inflammasome activation through the SHP2-JNK cascade, while also enhancing mitochondrial stability.

Mitochondrial fragmentation, a key feature of cellular stress, is characterized by reduced membrane potential and impaired respiratory function [20]. Furthermore, in established LPS-induced lung injury models, a compromised antioxidative defenses is associated with oxida-

tive damage, which culminates in mitochondria-induced apoptosis [21]. Considering the mitochondria's central role in cellular metabolism, their biogenesis and proper function are vital for the sustenance of lung epithelial cells. This study uncovers significant alterations in mitochondrial autophagy and its governing pathways during SALI. It is plausible that impaired mitochondrial autophagy, coupled with organelle dysfunction and pneumocyte death, may synergistically provoke inflammation and compromise respiratory capacity. These insights pave the way for novel understandings of mitochondrial dynamics in SALI, suggesting that interventions aimed at mitigating mitochondrial impairment in pulmonary tissue could offer significant therapeutic potential for SALI patients, pending future empirical clinical corroboration.

Prior investigations have established DUSP1 as a pivotal modulator of angiotensin II-mediated cellular responses, controlling three critical mitogen-activated protein kinase (MAPK) pathways: the extracellular signal-regulated kinase (ERK), c-Jun N-terminal kinase (JNK), and p38 [22]. Our recent experimental findings, ascertained through Western blot analysis, demonstrated that DUSP1 elevated SHP2 protein levels and its enzymatic function while concurrently suppressing the expression of p53 and JNK proteins following SHP2 activation. Considering that active JNK is known to promote mitochondrial autophagy, the role of SHP2 in this context, marked by PINK1 and Parkin, appears critical for reducing apoptotic events in alveolar epithelial cells.

Our research solidifies the functional connection between DUSP1 and SALI. The upregulation of DUSP1 preserves mitochondrial integrity, thereby mitigating the lung damage instigated by inflammatory processes. In light of DUSP1's established anti-inflammatory effects in various pulmonary conditions, it stands as a strong potential pharmacological candidate for novel treatments aimed at correcting dysregulated inflammatory responses in lung cells, with SHP2 now identified as a significant contributor to this protective mechanism. Synthesizing our findings, DUSP1 plays a pivotal role in diminishing the severity of alveolar damage during sepsis. The heightened expression of DUSP1 enhances mitochondrial autophagy, which in turn fortifies mitochondrial respiration and metabolic stability. By safeguarding mitochondrial integrity, DUSP1 promotes the viability of alveolar cells and curtails inflammatory responses, culminating in improved pulmonary function. In essence, our study proposes that DUSP1 orchestrates the modulation of the JNK/P53/NLRP3 signaling axis through the upregulation of SHP-2 expression and activity, thus impeding the progression of SALI.

Conclusion

This study establishes DUSP1 as a pivotal regulator of the cellular response to LPS-induced inflammatory lung injury. Functionally, our findings demonstrate that DUSP1 confers comprehensive cytoprotection by mitigating oxidative stress, suppressing apoptosis, and dampening the release of pro-inflammatory cytokines. Mechanistically, we reveal that DUSP1 exerts its regulatory function through a direct interaction with the protein tyrosine phosphatase SHP2. This binding subsequently suppresses the downstream activation of the JNK signaling pathway, which in turn enhances mitochondrial stability via the coordinated inhibition of both mitophagy and pro-apoptotic signaling. Collectively, these findings illuminate a novel protective mechanism and position DUSP1 as a promising therapeutic candidate for the future management of ALI and sepsis-associated pulmonary dysfunction.

Acknowledgements

This study was supported by the Natural Science Foundation of Fujian Province (grant numbers: 2021J01786). Supporting for Top Hospital and Specialty Excellence of Fujian Province [grant numbers: 2022(884)].

Disclosure of conflict of interest

None.

Address correspondence to: Sheng Chen, Department of Cardiovascular Surgery, Fujian Medical University Union Hospital, 29 Xinquan Road, Gulou District, Fuzhou 350001, Fujian, China. Tel: +86-13365917660; E-mail: chensheng@fjmu.edu.cn

References

[1] Long ME, Mallampalli RK and Horowitz JC. Pathogenesis of pneumonia and acute lung injury. Clin Sci (Lond) 2022; 136: 747-769.

[2] Shi L, Zha H, Pan Z, Wang J, Xia Y, Li H, Huang H, Yue R, Song Z and Zhu J. DUSP1 protects

against ischemic acute kidney injury through stabilizing mtDNA via interaction with JNK. Cell Death Dis 2023; 14: 724.
[3] Zhou M, Meng L, He Q, Ren C and Li C. Valsartan attenuates LPS-induced ALI by modulating NF-κB and MAPK pathways. Front Pharmacol 2024; 15: 1321095.
[4] Wang X, Wu FP, Huang YR, Li HD, Cao XY, You Y, Meng ZF, Sun KY and Shen XY. Matrine suppresses NLRP3 inflammasome activation via regulating PTPN2/JNK/SREBP2 pathway in sepsis. Phytomedicine 2023; 109: 154574.
[5] Wang J, Pu X, Zhuang H, Guo Z, Wang M, Yang H, Li C and Chang X. Astragaloside IV alleviates septic myocardial injury through DUSP1-Prohibitin 2 mediated mitochondrial quality control and ER-autophagy. J Adv Res 2024; [Epub ahead of print].
[6] Pu X, Zhang Q, Liu J, Wang Y, Guan X, Wu Q, Liu Z, Liu R and Chang X. Ginsenoside Rb1 ameliorates heart failure through DUSP-1-TMBIM-6-mediated mitochondrial quality control and gut flora interactions. Phytomedicine 2024; 132: 155880.
[7] Jiang Z, Zhao Q, Chen L, Luo Y, Shen L, Cao Z and Wang Q. UBR3 promotes inflammation and apoptosis via DUSP1/p38 pathway in the nucleus pulposus cells of patients with intervertebral disc degeneration. Hum Cell 2022; 35: 792-802.
[8] Zhu G, Xie J, Kong W, Xie J, Li Y, Du L, Zheng Q, Sun L, Guan M, Li H, Zhu T, He H, Liu Z, Xia X, Kan C, Tao Y, Shen HC, Li D, Wang S, Yu Y, Yu ZH, Zhang ZY, Liu C and Zhu J. Phase separation of disease-associated SHP2 mutants underlies MAPK hyperactivation. Cell 2020; 183: 490-502, e418.
[9] Sun Z, Liu Q, Lv Z, Li J, Xu X, Sun H, Wang M, Sun K, Shi T, Liu Z, Tan G, Yan W, Wu R, Yang YX, Ikegawa S, Jiang Q, Sun Y and Shi D. Targeting macrophagic SHP2 for ameliorating osteoarthritis via TLR signaling. Acta Pharm Sin B 2022; 12: 3073-3084.
[10] An L, Huo Y, Xiao N, Su S and Wang K. SHP2 mediates the ROS/JNK/NFAT4 signaling pathway in gastric cancer cells prompting lncRNA SNHG18 to drive gastric cancer growth and metastasis via CAR-T cells. Heliyon 2024; 10: e34008.
[11] Gao X, Shao S, Zhang X, Li C, Jiang Q and Li B. Interaction between CD244 and SHP2 regulates inflammation in chronic obstructive pulmonary disease via targeting the MAPK/NF-κB signaling pathway. PLoS One 2024; 19: e0312228.
[12] Wang J, Fan Y, Cai X, Gao Z, Yu Z, Wei B, Tang Y, Hu L, Liu WT and Gu Y. Uric acid preconditioning alleviated doxorubicin induced JNK activation and Cx43 phosphorylation associated cardiotoxicity via activation of AMPK-SHP2 signaling pathway. Ann Transl Med 2020; 8: 1570.
[13] Li C, Ma D, Chen Y, Liu W, Jin F and Bo L. Selective inhibition of JNK located on mitochondria protects against mitochondrial dysfunction and cell death caused by endoplasmic reticulum stress in mice with LPS-induced ALI/ARDS. Int J Mol Med 2022; 49: 85.
[14] Sinha P, Kerchberger VE, Willmore A, Chambers J, Zhuo H, Abbott J, Jones C, Wickersham N, Wu N, Neyton L, Langelier CR, Mick E, He J, Jauregui A, Churpek MM, Gomez AD, Hendrickson CM, Kangelaris KN, Sarma A, Leligdowicz A, Delucchi KL, Liu KD, Russell JA, Matthay MA, Walley KR, Ware LB and Calfee CS. Identifying molecular phenotypes in sepsis: an analysis of two prospective observational cohorts and secondary analysis of two randomised controlled trials. Lancet Respir Med 2023; 11: 965-974.
[15] Liu Z, Wang J, Dai F, Zhang D and Li W. DUSP1 mediates BCG induced apoptosis and inflammatory response in THP-1 cells via MAPKs/NF-κB signaling pathway. Sci Rep 2023; 13: 2606.
[16] Vringer E and Tait SWG. Mitochondria and cell death-associated inflammation. Cell Death Differ 2023; 30: 304-312.
[17] Zhu M, Wang Y, Zhu L, Du S, Wang Z, Zhang Y, Guo Y, Tu Y and Song E. Crosstalk between RPE cells and choroidal endothelial cells via the ANXA1/FPR2/SHP2/NLRP3 inflammasome/pyroptosis axis promotes choroidal neovascularization. Inflammation 2022; 45: 414-427.
[18] Qiu WQ, Ai W, Zhu FD, Zhang Y, Guo MS, Law BY, Wu JM, Wong VK, Tang Y, Yu L, Chen Q, Yu CL, Liu J, Qin DL, Zhou XG and Wu AG. Polygala saponins inhibit NLRP3 inflammasome-mediated neuroinflammation via SHP-2-Mediated mitophagy. Free Radic Biol Med 2022; 179: 76-94.
[19] Gong L, Shen Y, Wang S, Wang X, Ji H, Wu X, Hu L and Zhu L. Nuclear SPHK2/S1P induces oxidative stress and NLRP3 inflammasome activation via promoting p53 acetylation in lipopolysaccharide-induced acute lung injury. Cell Death Discov 2023; 9: 12.
[20] Marchi S, Guilbaud E, Tait SWG, Yamazaki T and Galluzzi L. Mitochondrial control of inflammation. Nat Rev Immunol 2023; 23: 159-173.
[21] Zhang Y, Li T, Pan M, Wang W, Huang W, Yuan Y, Xie Z, Chen Y, Peng J, Li X and Meng Y. SIRT1 prevents cigarette smoking-induced lung fibroblasts activation by regulating mitochondrial oxidative stress and lipid metabolism. J Transl Med 2022; 20: 222.
[22] Han J, Liu X and Wang L. Dexmedetomidine protects against acute lung injury in mice via the DUSP1/MAPK/NF-κB axis by inhibiting miR-152-3p. Pulm Pharmacol Ther 2022; 102131.